Available online at www.sciencedirect.com
SCIENCE DIRECT®
Journal of Power Sources 117 (2003) 75–83
JOURNAL OF POWER SOURCES
www.elsevier.com/locate/jpowsour

# Power supply quality improvement with a SOFC plant by neural-network-based control

Francisco Jurado*

*Department of Electrical Engineering, University of Jaén, 23700 EUP Linares (Jaén), Spain*

Received 24 October 2002; accepted 3 February 2003

**Abstract**

This paper demonstrates the potential of a solid-oxide fuel cell (SOFC) to perform functions other than the supply of real power to the grid. These additional functions however require the use of an inverter. The flux-vector control is used very effectively for the control of this inverter, where the space-vector pulsewidth modulation (SVM) is implemented by neural networks (NNs). The results presented in the paper show the effect of the fuel cell on the voltage at the sensitive load point. The performance of the fuel cell was found to be excellent.


*Keywords:* Dynamic modeling; Power systems simulation; Solid-oxide fuel cell (SOFC)

## 1. Introduction

A solid-oxide fuel cell (SOFC) equipped with a pulsewidth modulation (PWM) inverter interface can be used to palliate power quality problems. The requirement is to have independent control over the real and reactive components of the power injected into the ac grid. Under these conditions, the distributed generator can be configured to behave as dynamic voltage restorer (DVR). A series winding, associated with an inverter fed from the dc bus, can be included in the installation to inject the voltages required to support the ac grid voltage at the point of coupling during voltage sags and swells. These are mostly the result of single-phase faults on adjacent feeders.

Because the response time of the inverter is <10 ms, it is not necessary to include its detailed model in the slow dynamic fuel cell system. It is assumed that power factor can be adjusted accordingly by the power conditioner.

However, what must be included in the model is the direct effect of this switching. In order to do so, the vector control strategy proposed in [1] has been simulated. It is a system that accepts commands in terms of real power $P$ and reactive power $Q$, and it executes them by means of several control loops.

Space-vector pulsewidth modulation (SVM) has recently become a very popular PWM method for voltage-fed converter ac machine drives because of its superior harmonic quality and extended linear range of operation. However, one difficulty of SVM is that it requires complex online computation that usually limits its operation up to several kilohertz of switching frequency. Of course, switching frequency can be extended by using a high-speed DSP and simplified algorithms including lookup tables. Lookup tables, unless very large, tend to reduce pulsewidth resolution.

In this paper, the SVM have been implemented by neural networks (NNs). Neural networks, in general, are showing very high promise for simplification of control and feedback signal processing [2–4].

The paper is structured as follows. Section 2 presents a review of the fuel cell model. Some basic concepts of the inverter control are presented in Section 3. Section 4 describes the architecture of NNs. Section 5 depicts some simulation results. Finally, conclusions are presented in Section 6.

## 2. Fuel cell model

There are several types of fuel cells being developed for a variety of applications [5,6] and these have been extensively discussed in the open literature. Unlike other variants, the SOFC is entirely solid state with no liquid components. Operation at elevated temperature is needed to achieve the necessary level of conductivity in the cell's solid electrolyte for it to operate efficiently. With an outlet temperature in the range of 900–1000 °C, the efficiency of the cell alone is about 50%.

* Tel.: +34-953-026518; fax: +34-953-026508.
*E-mail address:* fjurado@ujaen.es (F. Jurado).

0378-7753/03/$ – see front matter 
doi:10.1016/S0378-7753(03)00309-4

**Nomenclature**

*Fuel cell*

| | |
|---|---|
| $E_0$ | ideal standard potential |
| $F$ | Faraday's constant |
| $I_{fc}$ | fuel cell current |
| $K_{H_2}$ | valve molar constant for hydrogen |
| $K_{H_2O}$ | valve molar constant for water |
| $K_{O_2}$ | valve molar constant for oxygen |
| $K_r$ | constant, $K_r = N_0/4F$ |
| $N_0$ | number of cells in series in the stack |
| $p_i$ | partial pressure |
| $P$ | real power |
| $P^*$ | set point for the real power |
| $q_{fc}^{in}$ | input fuel flow |
| $q_{fc}^{r}$ | fuel flow that reacts |
| $r$ | ohmic loss |
| $r_{H-O}$ | ratio of hydrogen to oxygen |
| $R$ | universal gas constant |
| $T$ | absolute temperature |
| $T_e$ | electrical response time |
| $T_f$ | fuel processor response time |
| $U_{opt}$ | optimal fuel utilization |
| $V_{fc}$ | fuel cell voltage |
| $\tau_{H_2}$ | response time for hydrogen flow |
| $\tau_{H_2O}$ | response time for water flow |
| $\tau_{O_2}$ | response time for oxygen flow |

*Inverter*

| | |
|---|---|
| $\boldsymbol{E}$ | load bus voltage |
| $\boldsymbol{E}^*$ | set point for the load bus voltage |
| $Q$ | reactive power |
| $Q^*$ | set point for the reactive power |
| $\boldsymbol{V}$ | inverter output voltage space-vector |
| $\delta_p$ | angle between $\psi_v$ and $\psi_e$ |
| $\delta_p^*$ | angle reference |
| $\psi_e$ | flux-vector associated with $\boldsymbol{E}$ |
| $\psi_v$ | flux-vector associated with $\boldsymbol{V}$ |
| $\psi_v^*$ | flux-vector reference |

*Neural networks*

| | |
|---|---|
| $f_{s\omega}$ | switching frequency |
| $f(\psi_v^*)$ | voltage magnitude function |
| $g(\alpha^*)$ | pulsewitdh function of a phase at unit voltage amplitude |
| $T_{A\text{-on}}$ | turn-on time of the phase A |
| $T_s$ | sampling time, $T_s = 1/f_{s\omega}$ |

Typically, the fuel cell system consists of SOFC generator modules in a parallel flow arrangement, with the number of standard modules being determined by the plant power requirement. The SOFC generator module embodies a number of tubular cells, which are combined to form cell bundle rows, several of which are arranged side by side to make up the complete assembly.

The high efficiency of the system means that less carbon dioxide is generated than in contemporary power plants. In addition, the fuel is oxidized electrochemically without any interaction with atmospheric nitrogen so negligible amounts of nitrogen oxide are discharged to the environment.

Models for simulating fuel cell based plants have been developed by Bessette [7], Haynes [8], Padullés [9], Massardo [10], Campanari [11], and Rao [12].

This paper provides a basic SOFC power section dynamic model used for performance analysis during normal operation. Some control strategies of the fuel cell system, response functions of fuel processor and power section are combined to model the SOFC power generation system.

The chemical response in the fuel processor is usually slow. It is associated with the time to change the chemical reaction parameters after a change in the flow of reactants. This dynamic response function is modeled as a first-order transfer function with a 5 s time constant.

The electrical response time in the fuel cells is generally fast and mainly associated with the speed at which the chemical reaction is capable of restoring the charge that has been drained by the load. This dynamic response function is also modeled as a first-order transfer function but with a 0.8 s time constant.

With aid of the power conditioner, the fuel cell system can supply not only real power but also reactive power. Usually, power factor can be in the range of 0.8–1.0. The SOFC system dynamic model is given in Fig. 1.

## 3. Utility-connected inverter control

Essentially, inverter flux-vector control involves appropriately choosing the inverter voltage vectors, so as to make the flux follow a reference flux-vector within a specified tolerance band.

Because the modulator does not directly control the load, the response of the load quantities is not as fast. However, the advantage here is that it does lead to a general-purpose modulator whose task is to control the inverter flux-vector to whatever value is specified by the outer control loop. The outer control loop can then be designed independently to generate the inverter flux-vector set point for achieving the desired final result.

Inverter flux-vector control can be used very effectively for the control of inverters which have their outputs connected to the main utility system. This section describes the flux control of a three-phase inverter connected to the utility system through a sine-wave output filter. The control system for the inverter is given in Fig. 2.

The instantaneous position of the rotating $q$–$d$ reference frame axes is determined relative to the utility mains voltage, either by the use of a phase-locked loop (PLL) or by the use of a power–frequency droop characteristic as in [1]. In either case, in the steady state, the $q$–$d$ frame angular frequency

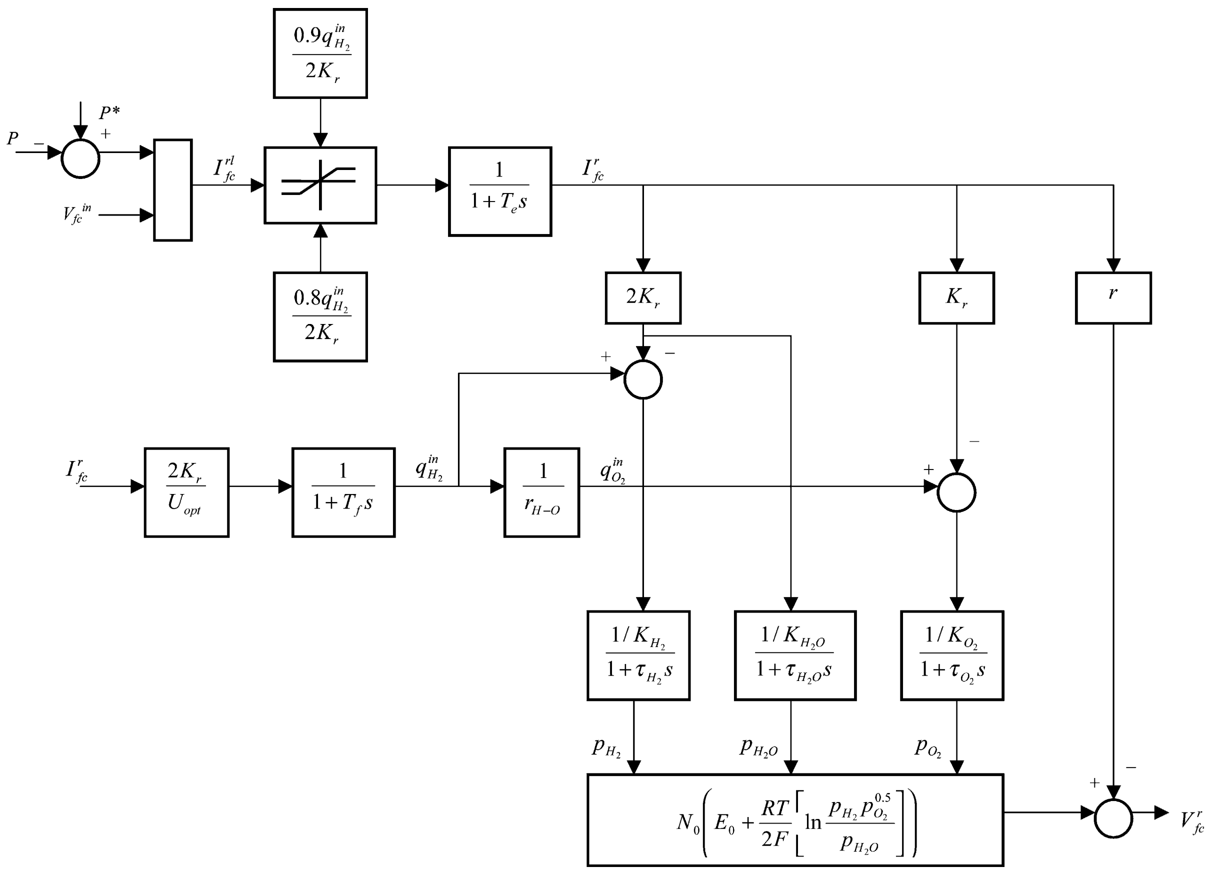


Fig. 1. SOFC system dynamic model.

equals the mains frequency, and its position relative to the mains voltage determines the sharing of the total load power between the inverter and the utility mains.

The inverter controller is required to align the filtered output voltage vector $\boldsymbol{E}$ with the rotating $q$ axis of the reference frame. The inverter flux-vector $\psi_\mathrm{v}$ can be used as a very effective forcing quantity to achieve this.

Further, being a continuous quantity, it is very convenient to use the flux-vector to define the power angle, which essentially determines the flow of real power from the inverter to the load bus. In Fig. 3, this is the angle between the vectors $\psi_\mathrm{v}$ and $\psi_\mathrm{e}$, where $\psi_\mathrm{e}$ is the flux-vector associated with the load bus voltage $\boldsymbol{E}$.

The inverter flux-vector $\psi_\mathrm{v}$ is the forcing quantity, used to align the filtered voltage vector with the rotating axis, and ensure that it has the desired magnitude.

To force the filtered voltage vector $\boldsymbol{E}$ to assume the desired value $\boldsymbol{E}^*$, the inverter flux-vector reference $\psi_\mathrm{v}^*$ can be generated by a proportional–integral (PI) controller acting on the voltage vector error $\varepsilon = \boldsymbol{E}^* - \boldsymbol{E}$, in the rotating reference frame:

$$\psi_\mathrm{v}^* = k_\mathrm{p}\varepsilon + k_\mathrm{i}\int \varepsilon\,\mathrm{d}t \tag{1}$$

In this equation, the complex constants $k_\mathrm{p}$ and $k_\mathrm{i}$ are the gains of the rotating frame vector PI controller.

For the purpose of controller design, it is assumed that the inverter, as controlled by the flux modulator, is capable of producing the commanded flux-vector at its output with negligible delay. That is, the assumption that $\psi_\mathrm{v} = \psi_\mathrm{v}^*$ is always valid.

## 4. Neural networks

Most real life physical systems are actually non-linear systems. The NN is an universal estimator. This implies that the NN can be trained to approximate any smooth non-linear function with accuracy. The ability of NNs to approximate non-linear functions relating input–output data from a non-linear system explains the increasing attention that they are attracting as candidates for novel control systems.

The PWM controller receives the $\psi_\mathrm{v}^*$ and $\delta_\mathrm{p}^*$ signals at the input and translates to gate drive signals for the insulated gate bipolar transistor (IGBT) inverter. The terminal voltages and currents are sensed, filtered by low-pass filters. Fig. 4 shows the topology of the neural-network-based SVM. It receives the $\psi_\mathrm{v}^*$ and $\delta_\mathrm{p}^*$ signals at the input and generates symmetrical pulses for three phases at the output, as shown in the figure.

Basically, the network consists of two subnets: the magnitude subnet (shown in the upper part) which implements

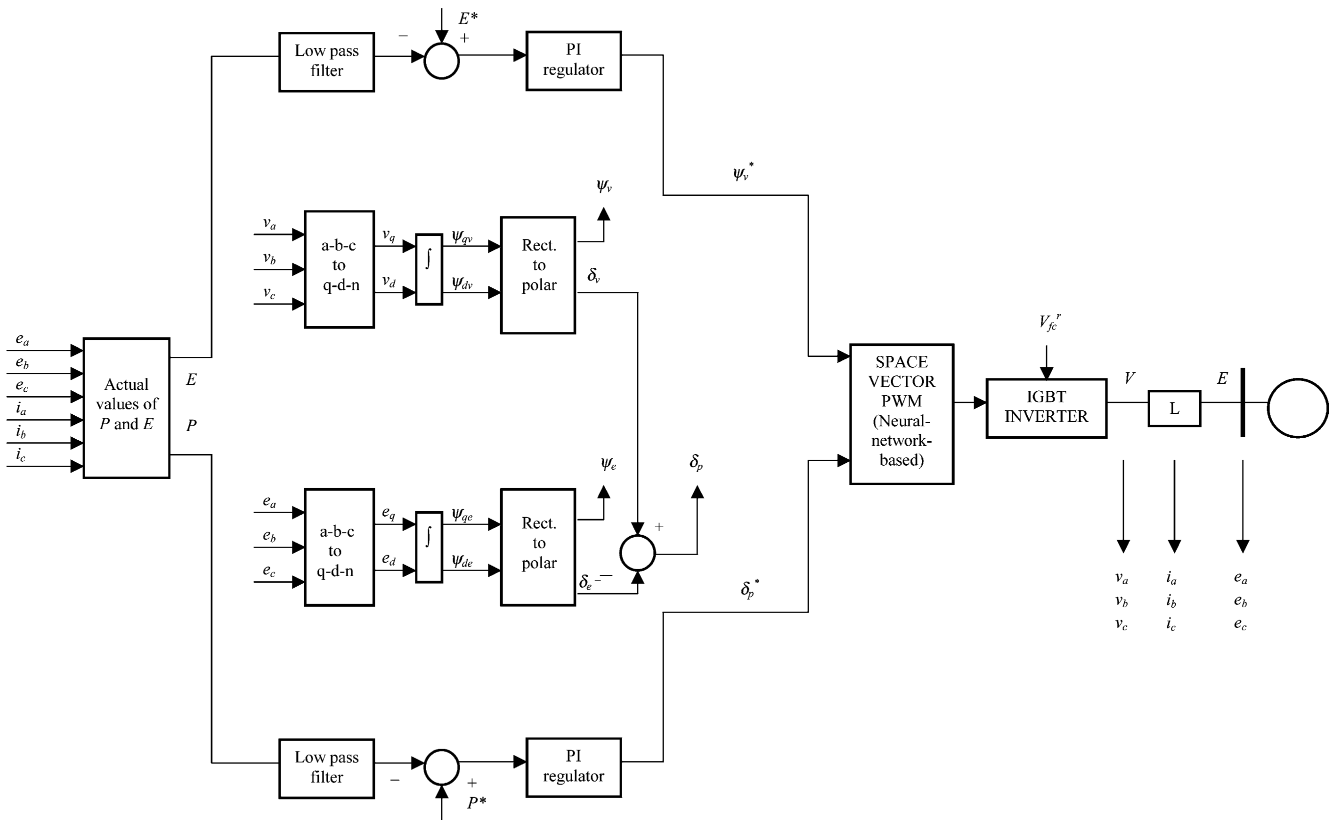


Fig. 2. Control system for the inverter.

the function $f(\psi_v^*)$ which is linear in the undermodulation region but nonlinear in the overmodulation region; and the angle subnet implements the pulsewidth function $g(\alpha^*)$ for the three phases at phase shift angles of $2\pi/3$ [13,14]. Note that the sigmoidal activation functions of the angle subnet generate only unipolar outputs, and these are converted to bipolar outputs by adding a fixed bias in the denormalization process. The digital words corresponding to turn-on time ($T_{on}$) of the phase A can be expressed as:

$$T_{A-on} = f(\psi_v^*) g_A(\alpha^*) + \tfrac{1}{4} T_s \tag{2}$$

For the symmetrical pulsewidth of each phase, the turn-off time can be given in the form:

$$T_{off} = T_s - T_{on} \tag{3}$$

The training data were generated by simulation of a conventional SVM algorithm, and then a backpropagation technique in the MATLAB-based Neural Network Toolbox [15] was used for offline training. In the NN-based SVM technique, the digital words corresponding to turn-on time are generated by the network and then converted to pulsewidths by a single timer.

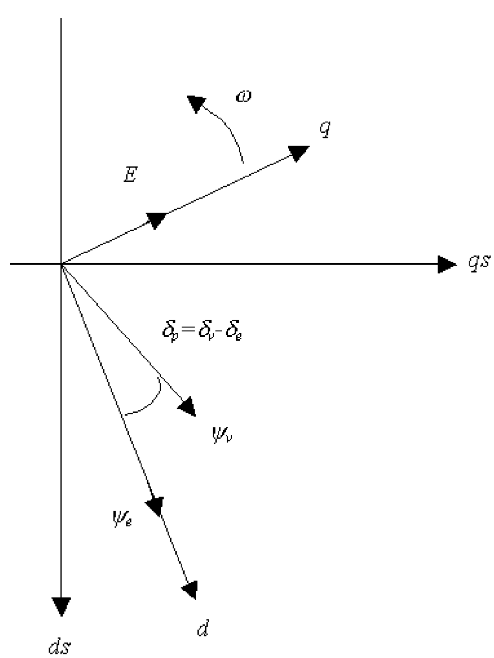


Fig. 3. Flux-vector diagram of inverter.

## 5. Results

Fig. 5 shows the test system used to carry out the various simulations. The majority of data for the fuel cell model has been extracted from [16,17], and a commercial leaflet describing a SOFC 100 kW plant.

The total simulation period is 0.5 s. Using the facilities available in MATLAB, the fuel cell plant is simulated to be in operation, as it is expected to be the case in a practical

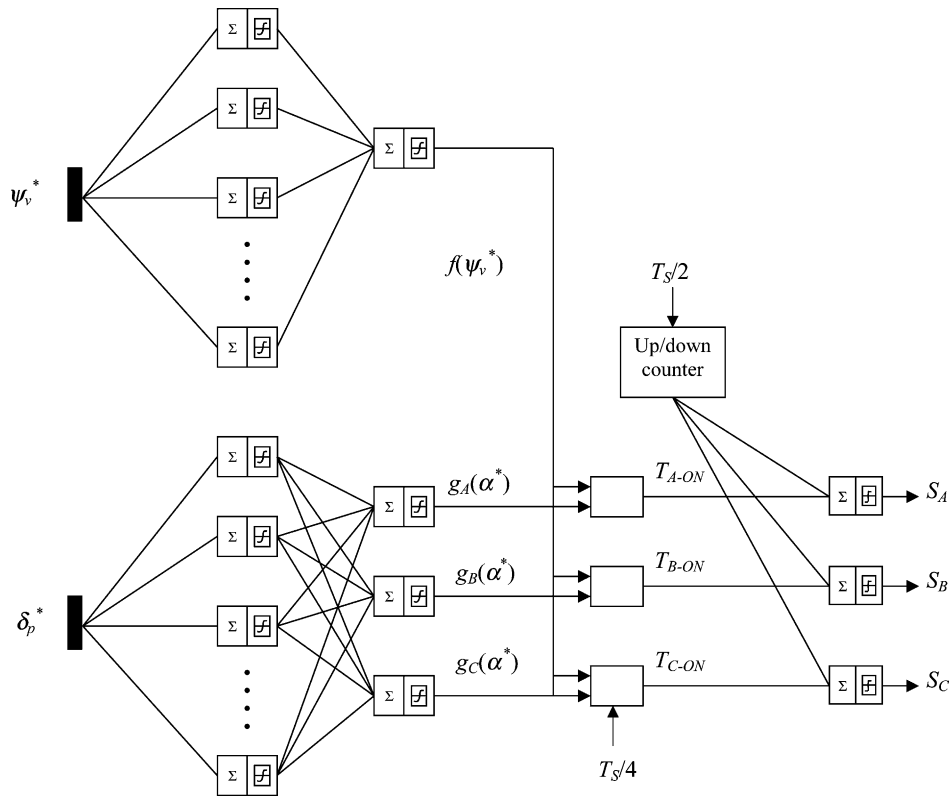


Fig. 4. Topology of neural-network-based SVM modulator.

situation. The results for the simulations are shown in Figs. 6–11.

In each figure, the first simulation contains no fuel cell plant. The second simulation is carried out using the same scenario as above, but now with the fuel cell plant in operation.

Different transformer winding connections between the fault location and load terminal will cause different sags at

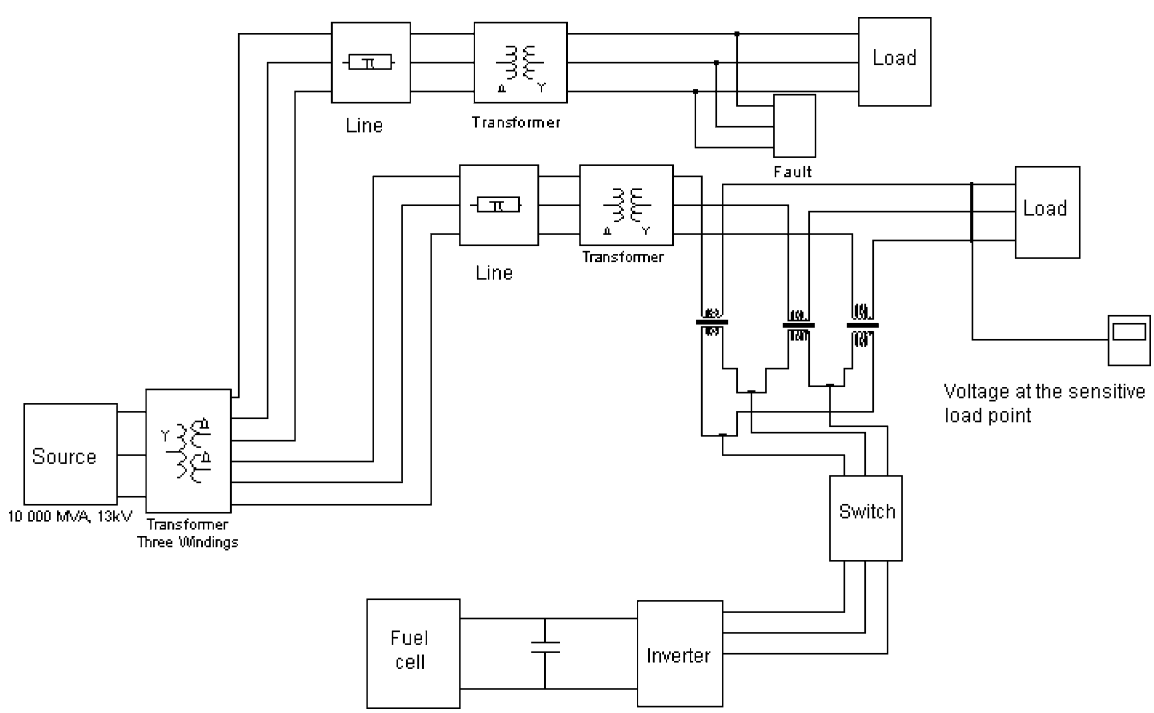


Fig. 5. Test system implemented in MATLAB to carry out the simulations.

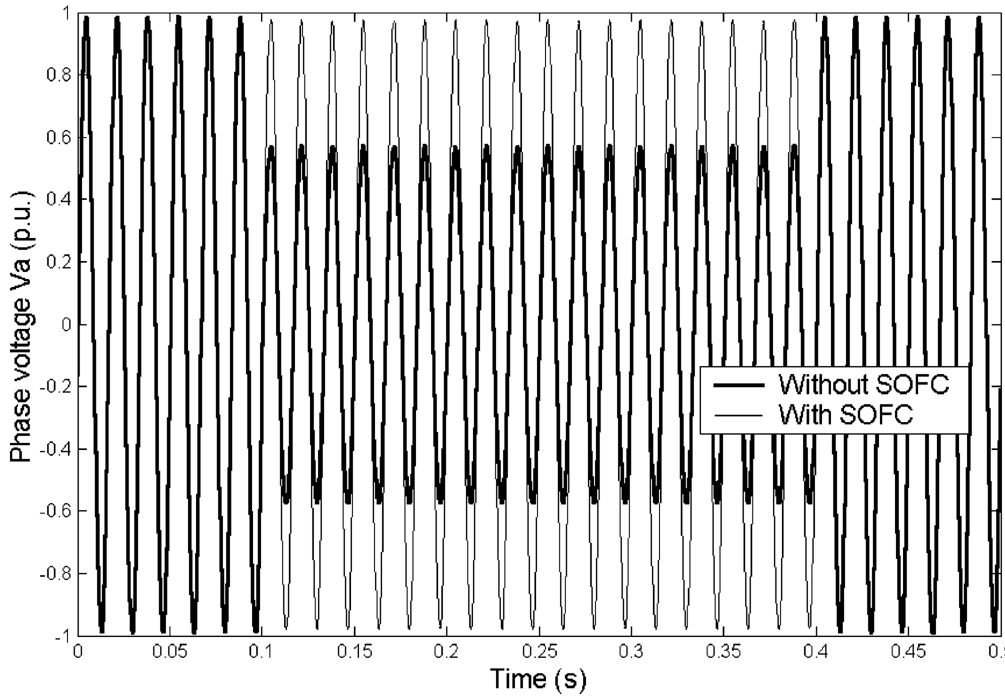


Fig. 6. Phase voltage at the sensitive load point in Fig. 5 due to an SLGF.

the load terminal due to imbalanced faults. Transformers with winding connections of $\Delta/Y$, $Y/\Delta$ will result in the same sag at the load terminal. This consists of a large voltage drop on two phases and a relatively small drop on the third phase.

The transformer winding connections between the point of the fault and the equipment terminals swap the three-phase voltages in case of an imbalanced sag.

Most of the faults on the utility transmission and distribution systems are single line-to-ground faults (SLGFs). An SLGF on the primary side of a $\Delta/Y$ or $Y/\Delta$ transformer will change into a phase-to-phase fault on the secondary side [18]. Fig. 6 shows the phase voltage at the sensitive load point, due to an SLGF of 18 cycles on phase A.

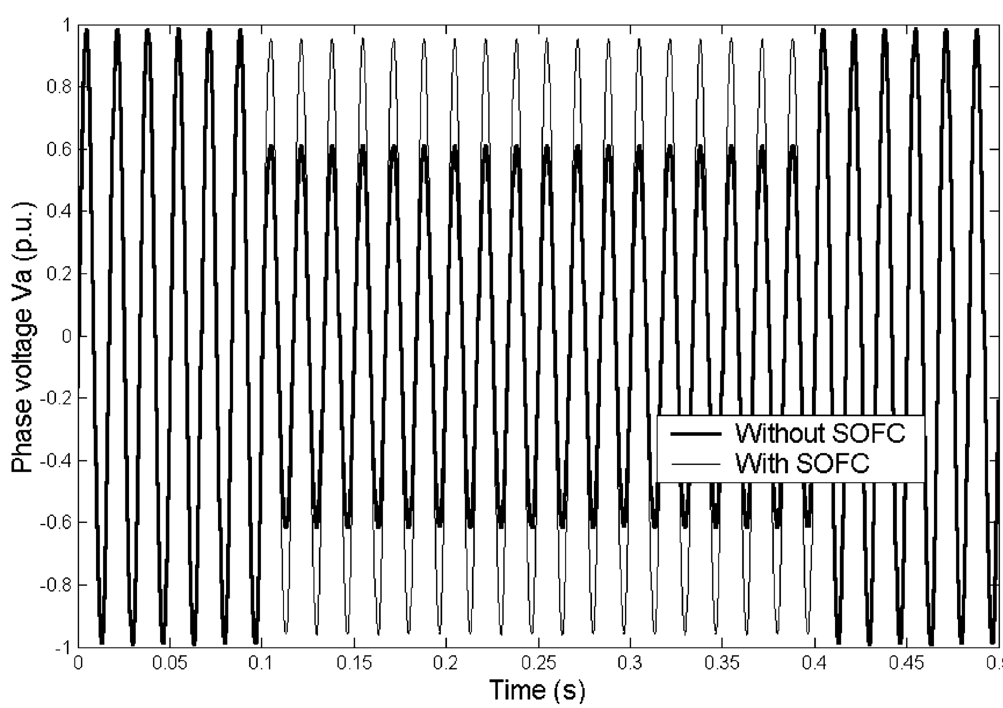


Fig. 7. Phase voltage at the sensitive load point in Fig. 5 due to an LLF on phase A.

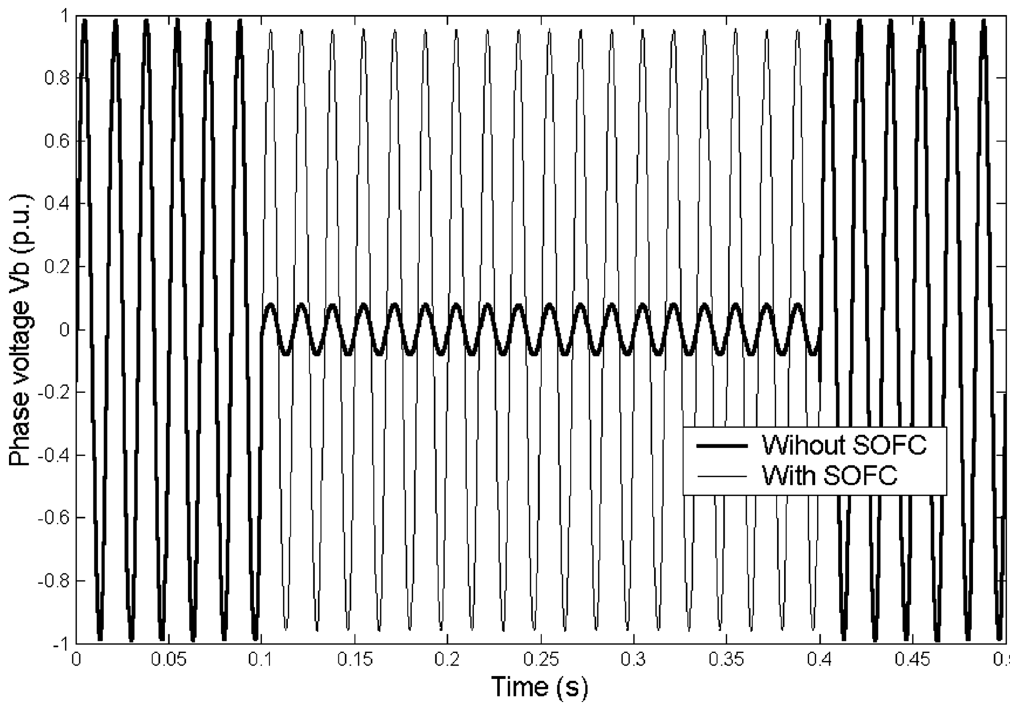


Fig. 8. Phase voltage at the sensitive load point in Fig. 5 due to an LLF on phase B.

Line-to-line faults (LLFs) on the primary side of the transformer cause similar types of sag as SLGFs, but with lower voltage magnitude at the load terminal.

One of the phase voltages drops almost to zero, while the other two phase voltages drop to around 60% of prefault voltage, as shown in Figs. 7 and 8. The fault is placed between lines B and C.

Fig. 9 depicts the voltage sag on phase A at the sensitive load point in Fig. 5 due to a three-phase fault of 300 ms duration. The voltage sag at the load point is 50% with respect to the reference voltage.

Fig. 10 shows the voltage sag on phase A in Fig. 5 due to a three-phase fault of 200 ms duration, and induction motors of 60%. Fig. 11 depicts the voltage sag and induction

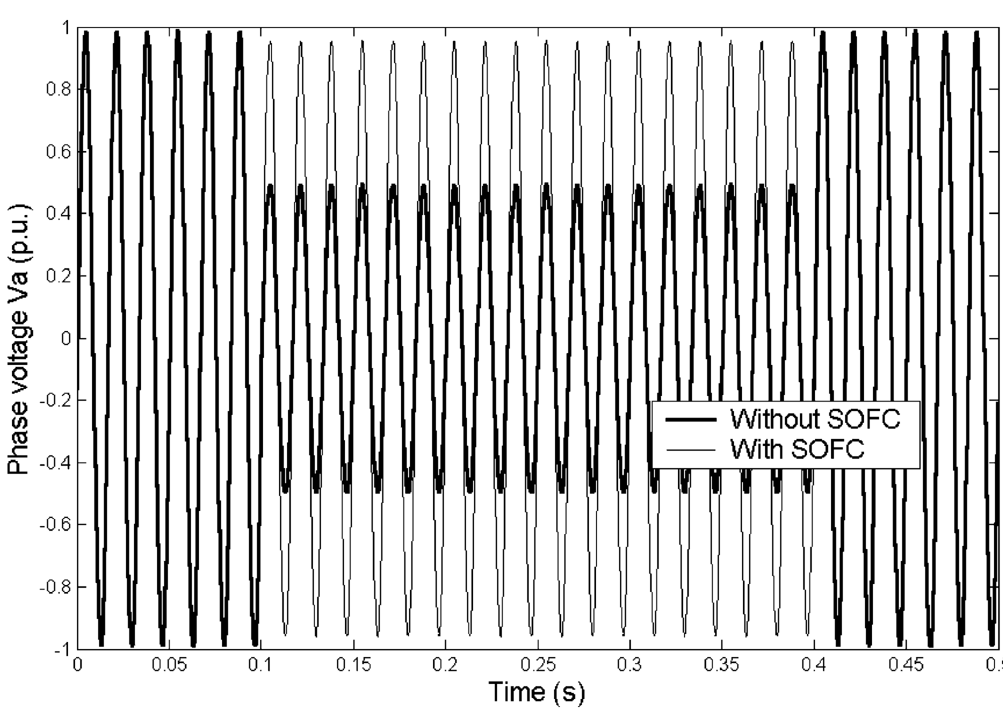


Fig. 9. Phase voltage at the sensitive load point in Fig. 5 due to a three-phase fault.

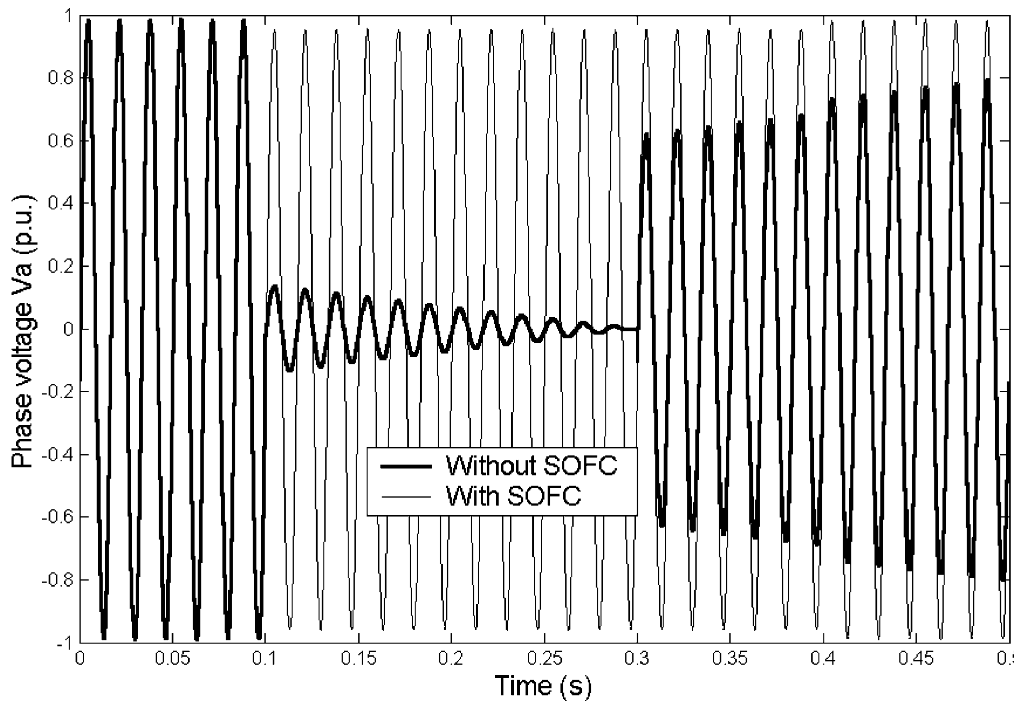


Fig. 10. Phase voltage at the sensitive load point in Fig. 5 due to a three-phase fault. Induction motors of 60%.

motors of 65%. These figures show the influence of induction motors on the shape and the duration of voltage sags.

Since it is a balanced fault, voltages in three phases are, therefore, the same, and phases B and C are not shown here. The voltage sag consists of a severe during-fault sag, directly due to the fault; and a less severe post-fault sag with longer duration, due to the induction motor reacceleration. The during-fault sag decays to zero in a few cycles.

An induction motor generally slows down, with energy being returned to the supply under generator action, during a fault. It simply operates as a generator for a short period and causes a decrease in sag. However, its reacceleration after fault clearance results in an extended post-fault [19].

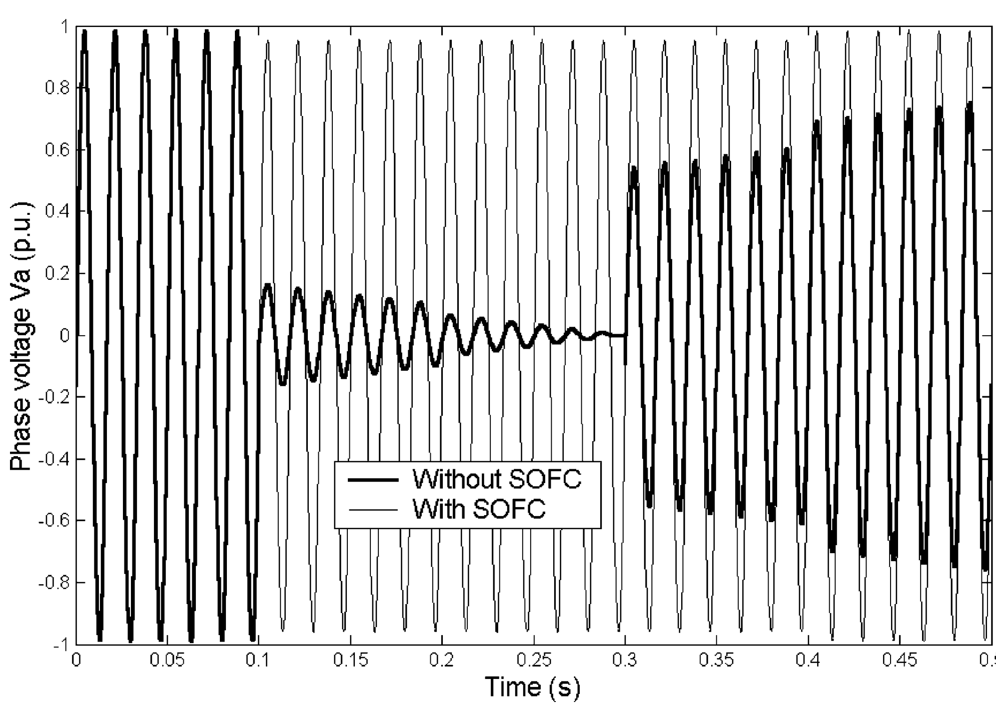


Fig. 11. Phase voltage at the sensitive load point in Fig. 5 due to a three-phase fault. Induction motors of 65%.

## 6. Conclusions

Conventional design approaches use different approximation methods to handle non-linearity. Some typical choices are, linear, piecewise linear, and lookup table approximations.

A linear approximation technique is relatively simple, however it tends to limit control performance and may be costly to implement in certain applications. A piecewise linear technique works better, although it is tedious to implement because it often requires the design of several linear controllers. A lookup table technique may help improve control performance, but it is difficult to debug and tune. Furthermore in complex systems where multiple inputs exist, a lookup table may be impractical or very costly to implement due to its large memory requirements.

Therefore, in this paper a non-linear controller is more suitable than the linear type since the SOFC equipped with a PWM inverter interface is truly a non-linear system.

Neural-network-based control can offer a superior performance and a better trade-off between system robustness and sensitivity, which results into handling non-linear control better than traditional methods.

This paper discusses the potential of fuel cell plants for enhancement of power quality. In particular, fuel cell plants can serve locally as voltage support of the ac bus.

Voltage sag is a significant disturbance, which may lead to tripping and high cost to sensitive customers. When the fuel cell plant is in operation the voltage sag is mitigated almost completely, and the voltage at the sensitive load point is maintained, as demonstrated by the examples given in this paper.

## References


[1] M.C. Chandorkar, D.M. Divan, R. Adapa, Control of parallel connected inverters in stand-alone ac supply systems, IEEE Trans. Ind. Appl. 29 (1) (1993) 136–143.

[2] M.P. Kazmierkowki, D.L. Sobczuk, M.A. Dzleniakowski, Proceedings of EPE Conference on Neural Network Current Control of VS-PWM Inverters, 1995, pp. 415–1420.

[3] J.M. Carrasco, J.M. Quero, F.P. Ridao, M.A. Perales, L.G. Franquelo, Sliding mode control of a dc/dc PWM converter with PFC implemented by neural networks, IEEE Trans. Circuits Syst. I 44 (8) (1997) 743–749.

[4] R. Leyva, L. Martinez-Salamero, B. Jammes, J.C. Marpinard, F. Guinjoan, Identification and control of power converters by means of neural networks, IEEE Trans. Circuits Syst. I 44 (8) (1997) 735–742.

[5] T. Moore, Market potential high for fuel cells, EPRI J. 22 (3) (1997) 6–17.

[6] The Future of Fuel Cells, Scientific American, 1999, pp. 72–83.

[7] N.F. Bessette, Modeling and simulation for solid oxide fuel cell power systems, Ph.D. thesis, Georgia Institute of Technology, 1994.

[8] C.L. Haynes, Simulation of tubular solid oxide fuel cell behavior for integration into gas turbine cycles, Ph.D. thesis, Georgia Institute of Technology, July, 1999.

[9] J. Padullés, G.W. Ault, J.R. McDonald, An integrated SOFC plant dynamic model for power systems simulation, J. Power Sources 86 (1–2) (2000) 495–500.

[10] A.F. Massardo, F. Lubelli, Internal reforming solid oxide fuel cell-gas turbine combined cycles (IRSOFC-GT). Part A. Cell model and cycle thermodynamic analysis, J. Eng. Gas Turbines Power 122 (27) (2000) 27–35.

[11] S. Campanari, Thermodynamic model and parametric analysis of a tubular SOFC module, J. Power Sources 92 (1–2) (2001) 26–34.

[12] A.D. Rao, G.S. Samuelsen, Analysis strategies for tubular solid oxide fuel cell based hybrid systems, J. Eng. Gas Turbines Power 124 (3) (2002) 503–509.

[13] J.O.P. Pinto, B.K. Bose, L.E. Borges, M.P. Kazmierkowski, A neural network based space vector PWM controller for voltage-fed inverter induction motor drive, IEEE Trans. Ind. Appl. 36 (6) (2000) 1628–1636.

[14] J.O.P. Pinto, B.K. Bose, L.E.B. da Silva, A stator flux oriented vector-controlled induction motor drive with space vector PWM and flux vector synthesis by neural networks, IEEE Trans. Ind. Appl. 37 (5) (2001) 1308–1318.

[15] Neural Network Toolbox User's Guide with MATLAB, Version 4, The Math Works Inc., Natick, MA, 2000.

[16] J.A. Kuipers, Proceedings of the 1998 Fuel Cell Seminar, 1998, 450 pp.

[17] S.C. Singhal, Progress in tubular solid oxide fuel cell technology, in: Proceedings of the Solid Oxide Fuel Cells, Honolulu, HI, USA, 17–22 October, 1999, pp. 39-51.

[18] M. Bollen, Understanding Power Quality Problems, Voltage Sags and Interruption, IEEE Press, New York, 1999.

[19] M. Bollen, The influence of motor reacceleration on voltage sags, IEEE Trans. Ind. Appl. 31 (4) (1995) 667–674.